UNIVERSITY *of* York

This is a repository copy of *Enhanced brightness of a laser-driven X-ray and particle source by microstructured surfaces of silicon targets*.

White Rose Research Online URL for this paper:
https://eprints.whiterose.ac.uk/160571/

Version: Published Version

Article:

White Rose
university consortium
Universities of Leeds, Sheffield & York

eprints@whiterose.ac.uk
https://eprints.whiterose.ac.uk/

Physics of Plasmas

Enhanced brightness of a laser-driven x-ray and particle source by microstructured surfaces of silicon targets

Tina Ebert (ID), Nico W. Neumann, Leonard N. K. Döhl, Jonathan Jarrett, Christopher Baird (ID), Robert Heathcote, Markus Hesse (ID), Aasia Hughes, Paul McKenna (ID), David Neely, Dean Rusby, Gabriel Schaumann (ID), Christopher Spindloe (ID), Alexandra Tebartz, Nigel Woolsey, and Markus Roth

View Online   Export Citation   CrossMark

ARTICLES YOU MAY BE INTERESTED IN

Target normal sheath acceleration by fs laser and advanced carbon foils with gold films and nanoparticles
Physics of Plasmas 27, 043107 (2020); https://doi.org/10.1063/5.0004834

Ionization and acceleration of multiply charged gold ions in solid film irradiated by high intensity laser
Physics of Plasmas 27, 033108 (2020); https://doi.org/10.1063/1.5140493

Enhancement of proton acceleration and conversion efficiency by double laser pulses plasma interactions
Physics of Plasmas 27, 033107 (2020); https://doi.org/10.1063/1.5143344

Enhanced brightness of a laser-driven x-ray and particle source by microstructured surfaces of silicon targets

Tina Ebert,[1,a] Nico W. Neumann,[1] Leonard N. K. Döhl,[2] Jonathan Jarrett,[3] Christopher Baird,[2]
Robert Heathcote,[4] Markus Hesse,[1] Aasia Hughes,[4] Paul McKenna,[3] David Neely,[3,4] Dean Rusby,[3]
Gabriel Schaumann,[1] Christopher Spindloe,[4] Alexandra Tebartz,[1] Nigel Woolsey,[2] and Markus Roth[1]

AFFILIATIONS

[1]Institut für Kernphysik, Fachbereich Physik, Technische Universität Darmstadt, D-64289 Darmstadt, Germany
[2]York Plasma Institute, Department of Physics, University of York, York YO10 5DD, United Kingdom
[3]Department of Physics, Scottish Universities Physics Alliance, University of Strathclyde, Glasgow G4 0NG, United Kingdom
[4]Central Laser Facility, Science and Technology Facilities Council, Didcot OX11 0QX, United Kingdom

[a]Author to whom correspondence should be addressed: tebert@ikp.tu-darmstadt.de

ABSTRACT

The production of intense x-ray and particle sources is one of the most remarkable aspects of high energy laser interaction with a solid target. Wide application of these laser-driven secondary sources requires a high yield, which is partially limited by the amount of laser energy absorbed by the target. Here, we report on the enhancement of laser absorption and x-ray and particle flux by target surface modifications. In comparison to targets with flat front surfaces, our experiments show exceptional laser-to-target performance for our novel cone-shaped silicon microstructures. The structures are manufactured via laser-induced surface structuring. Spectral and spatial studies of reflectance and x-ray generation reveal significant increases of the silicon K_α line and a boost of the overall x-ray intensity, while the amount of reflected light decreases. Also, the proton and electron yields are enhanced, but both temperatures remain comparable to those of flat foil targets. We support the experimental findings with 2D particle in cell simulations to identify the mechanisms responsible for the strong enhancement. Our results demonstrate how custom surface structures can be used to engineer high power laser-plasma sources for future applications.

Published under license by AIP Publishing. https://doi.org/10.1063/1.5125775

I. INTRODUCTION

The interaction of ultra-intense high power laser pulses with matter is a dynamically growing field of interest.[1–3] The need for powerful, compact, and reliable high energy particle and radiation sources is an ongoing motivation for new techniques and materials within this field. One approach to improve these sources is using nano- and microstructured targets. Previous studies have shown that these targets can enhance absorption and specular reflectivity,[4] heating of electrons,[5] acceleration of ions,[6] and generation of bright x-ray radiation.[7] In particular, producing a brilliant x-ray source with high photon flux is a key motivation for further development into the potential applications of laser-plasma science and for improving experimental diagnostic techniques such as Thomson scattering,[8] x-ray backlighting,[9] and time-resolved x-ray spectroscopy.[10] In addition, an enhanced yield and distribution of highly energetic electrons are likely to improve the generation and acceleration of ions.

A large part of research in this field focuses on the so-called nanowire targets.[5,11,12] For this kind of target, high contrasts ($>10^{10}$) are required to achieve the best performance. Nevertheless, an enhancement compared to flat targets can also be attained with a lower contrast, but in this case, the effect is due to a long gradient preplasma. Here, problems can arise due to the filamentation of the low density plasma, which lowers the flux and maximum particle energy.[13] Additionally, according to Andreev *et al.*,[14] the pulse length should not exceed several tens of femtoseconds to achieve optimal performance. However, under comparable conditions, longer pulse durations ($\sim$ps) achieve higher accelerated particle energies and fluxes.[15] By using larger front surface structures, the preplasma gradient can be controlled more tightly, while the durability of the structures during laser interaction will be increased as well.

Several studies discuss the influence of the microstructure shape on laser target coupling.[4,16] In both cases, triangular structures achieve

excellent results. So far, to our understanding, this kind of structure has not been investigated experimentally.

Silicon surfaces can be modified to feature cone-like structures with high aspect ratios. They have highly light absorbing properties and are also referred to as "black silicon." In 1998, Her et al.[17] demonstrated the manufacturing process via ultrashort pulse laser processing in a sulfur hexafluoride (SF_6) atmosphere. A number of experiments and further developments[18] toward applications in photoelectrical and photochemical performances[19] have been demonstrated with different structural parameters[20] and a variety of materials.[21] The increased absorptance of microstructured silicon is achieved by the geometric trapping of light in the cone-like structures with pointed tips. Also, laser-driven doping of the silicon surface layer with sulfur atoms influences the process. Combining the two attributes results in an increase in the light absorption by more than 90% for the visible and near-infrared spectrum, above and below the bandgap of silicon.[22] While being straightforward to manufacture and customize the microstructure shape with existing equipment in target fabrication, the time needed to produce such a target is only in the range of several tens of seconds to a few minutes. Therefore, this proven technique is a flexible and efficient way to produce a large number of different targets in a very short time, which enables the use in higher repetition rate experiments to study the influence of this specific kind of microstructure in high intensity laser-matter interactions.

In this work, we compare these microstructured silicon targets to flat silicon foils in a laser plasma experiment in terms of emitted particles and radiation. The microstructures are located on the laser irradiated (front) surface, while the back side is polished flat. We observe a strong enhancement in absorptance of laser energy by the target, which in turn influences the generation of hot electrons, ions, and x-ray radiation. The experimental results are complemented with 2D particle in cell (PIC) simulations to interpret the underlying physics. In contrast to structures on the nanometer scale, the microstructures are expected to remain effective for more than a few hundred femtoseconds. To our knowledge, this is the first time silicon targets with cone-like microstructures have been used for improving high power laser to target coupling.

II. EXPERIMENTAL SETUP

A thorough comparison between flat monocrystalline silicon foils with a thickness of $25 \, \mu m$ and microstructured targets was performed within an identical setup. The microstructures were cone-shaped with a height of $15 \, \mu m$ and a base width of $5 \, \mu m$. The substrate thickness was approximately $5 \, \mu m$. An image of the structures is shown in the inset of Fig. 1.

The microstructured targets were produced by repetitive femtosecond laser pulse irradiation in a sulfur hexafluoride ambience at the Detector and Target Laboratory, Institut für Kernphysik, Technische Universität Darmstadt, as initially described by Her et al.[17] The
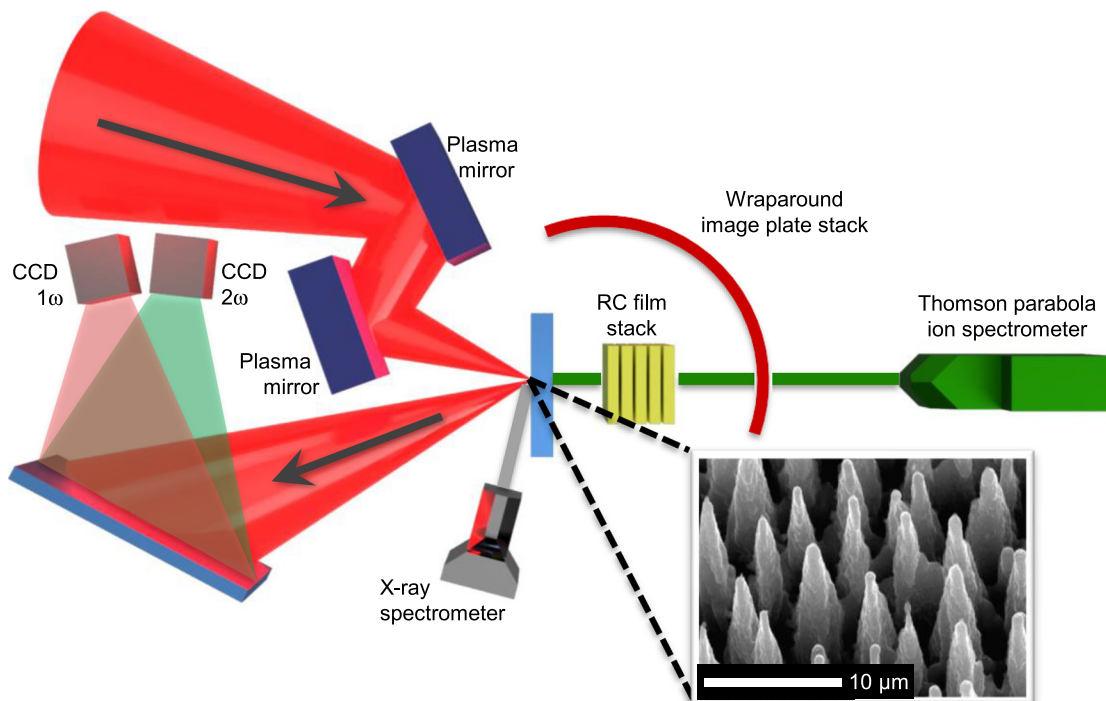
FIG. 1. Schematic illustration of the experimental setup. The experiment was performed using the Vulcan Petawatt Laser (Central Laser Facility, UK). The temporal laser contrast was increased to 10^{11} by using a double plasma mirror system. The incident angle between the laser and the target with respect to target normal is $20°$. Reflected and emitted light from the target front surface is collected via a ground glass scattering screen by two cameras for fundamental and second harmonic radiation. In addition, a conical KAP (potassium acid phthalate) x-ray spectrometer is aligned to the target front. On the target back side, a radiochromic film (RCF) stack and a Thomson parabola ion spectrometer, as well as a wraparound image plate stack for measuring the electron emission, are positioned. Inset: Scanning electron microscopy recording of the front surface of a microstructured silicon target, as used within the experimental campaign.

applied fabrication method is described in more detail in a publication by Ebert *et al.*[23] Here, an ambient pressure of 800 mbar (SF_6), a laser fluence of $10 \, kJ \, m^{-2}$, a focus diameter (Gaussian) of $60 \, \mu m$ (e^{-2}), and a scanning speed of $0.5 \, mm \, s^{-1}$ were applied to achieve the structural dimensions of the micro-cones.

A comprehensive experiment was conducted at the Central Laser Facility located at the STFC Rutherford Appleton Laboratory, UK. The Target Area Petawatt with a high power VULCAN laser system[24] offers ideal conditions to investigate the characteristics of novel and innovative target designs.

The laser energy delivered on target was (160 ± 30) J with a pulse length of (1.0 ± 0.1) ps (FWHM) and a focus diameter of $(10 \pm 2) \, \mu m$ (e^{-2}). This resulted in a peak intensity of $I_f = (2.0 \pm 0.1) \times 10^{20} \, W \, cm^{-2}$ for the flat targets. With an average of five structures in the focal spot and the given aspect ratio, the interaction area for the structured targets was increased by a factor of 7.5. Without considering the alterations of the topography by the expanding plasma, the peak intensity is therefore reduced down to $I_s = (2.8 \pm 0.7) \times 10^{19} \, W \, cm^{-2}$. The incident angle for the P-polarized beam (see Fig. 1) was $20°$ to target normal.

Because of the large laser incidence angle, it was possible to collect the light reflected from the target front surface on ground glass scattering screens. One screen, which covered a solid angle of 0.84 sr, was placed on-axis to monitor the reflected laser energy. The spatial distribution on the on-axis screen was recorded with two bandpass filtered CCD cameras. Hence, the fundamental radiation ($\omega = 1053$ nm) as a calibrated measure of reflected light can be distinguished from frequency doubled light ($\omega_{SHG} = 527$ nm). In addition, x-ray radiation was measured with a conical KAP (potassium acid phthalate) crystal spectrometer based on a design proposed by Martinolli *et al.*[25] The spectral range was 1.65 keV–1.84 keV, which centers on the silicon K_α line and includes a number of higher ionization states. The spectrometer covered a solid angle of 5×10^{-3} sr with a field of view larger than the source size and used a combination of PET, aluminium-coated mylar, and beryllium foils as filter. The spectral resolution was $E/\Delta E = (1200 \pm 100)$. To record the signal, image plates of the type Fuji BAS-TR were used, which give the time integrated spectrum. On the target back side normal axis, a radiochromic film stack (RCF) and a Thomson parabola ion spectrometer for kinetic energies E_{kin} above 4 MeV were used to measure the spatial and spectral distributions of protons. For a selection of shots, a wraparound stack of image plates[26,27] was inserted to monitor the electrons escaping from the

target rearside, which was covering a solid angle of $120°$. Protons with energies below 21 MeV were stopped before reaching the image plate stack by adding a 0.9 mm thick Fe sheet as the first layer. All image plates were digitized with a FLA5100 scanner.

The experimental setup was designed to obtain as complete a picture as possible of the transfer of incident laser energy into the plasma and is depicted in Fig. 1. This included measuring the properties of incident, reflected, and scattered laser light, as well as the highly energetic particles and electromagnetic radiation emitted from the target. To observe the effects of the front structure interacting with the highest intensity of the laser pulse, the temporal intensity contrast of the laser system is critical. Any substantial flux of energy before the main pulse will dramatically alter (or destroy for small scale structures) the target structure and will result in a preheated target with significantly differing conditions. To probe the unaltered target structure and gain the best possible quantitative information in this experiment, a double plasma mirror[28] was used to decrease the pre-pulse intensity below the laser-induced damage threshold for silicon and thereby increase the laser contrast on target from 10^7 to 10^{11} at 500 ps prior to the peak of the pulse.

III. RESULTS

The experiment focused on comparing the absorption physics of targets with microstructured front surfaces, as described above, with flat targets. The complementary measurements by the individual diagnostics are summarized in Table I. The average signal for eight shots on flat targets and seven shots on structured targets is shown for all diagnostics measuring protons and electromagnetic radiation. The electron emission was averaged over three shots each for structured and flat foil targets. All values are given together with their standard deviation.

A. Reflected and back-scattered light

The CCD cameras monitoring the scattering screen measured a significant reduction in the fundamental reflectivity [1053 nm, see Fig. 2(a)] and second harmonic emission (527 nm) of the front surface of the microstructured targets compared to the flat foils. The measured 1053 nm signal reflected from the flat targets accounts to $20 \pm 3\%$ of the incident laser energy. When the microstructured targets are used, $6 \pm 1\%$ is reflected. In addition, the relative emission signal of frequency doubled 527 nm light decreases by a factor of ten for microstructured in comparison to flat targets. Since the generation of the

TABLE I. Measurements comparing flat and structured targets. For flat targets, the averaged signal over eight shots is presented, and for structured targets, seven shots are taken into account. Only the electron data were averaged over three shots each, and the photo-stimulated luminescence (PSL) is given for the second layer of the wraparound stack. The uncertainties shown are the standard deviations, which correspond to the variation in the measured signals for identical experimental parameters. The x-ray intensity is the integral over the whole spectral range covered by the spectrometer, and the K_α intensity is the integrated signal between 1.734 keV and 1.750 keV. For the proton data, only particles with energies greater than 4 MeV were considered.

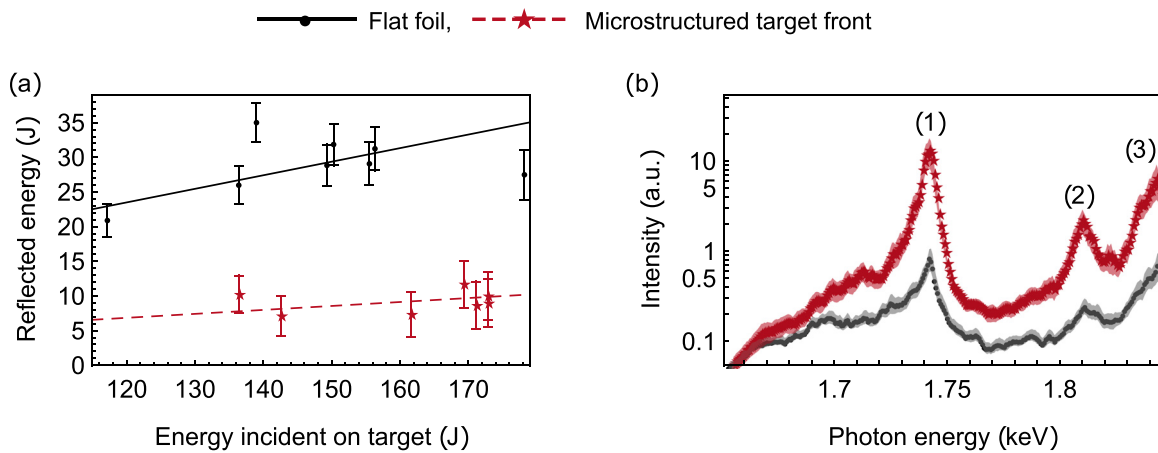|	Reflection 1053 nm (%)	Reflection 527 nm (arb. units)	X-ray intensity (keV sr^{-1}, $\times 10^{10}$)	K_α intensity (keV sr^{-1}, $\times 10^{10}$)	No. of electrons (PSL J^{-1})	Electron temp. (MeV)	No. of protons ($\times 10^{11}$)	Proton temp. (MeV)	Proton conversion efficiency (%)
Flat	20 ± 3	1.0 ± 0.5	0.54 ± 0.10	0.11 ± 0.01	21 ± 10	4 ± 1	4.3 ± 0.5	2.5 ± 0.1	0.27
Struct.	6 ± 1	0.10 ± 0.05	5.43 ± 1.30	1.3 ± 0.13	65 ± 22	4.6 ± 0.4	19 ± 1	2.36 ± 0.04	1.01
Ratio	$0.3\times$	$0.1\times$	$7.3\times$	$12\times$	$3.1\times$	$1.2\times$	$4.4\times$	$1.0\times$	$3.7\times$

FIG. 2. Diagnostic comparison of structured and flat silicon targets. (a) Reflection of fundamental radiation from the target front for 15 individual laser shots (eight flat and seven structured targets). The average signal for both target types is indicated by horizontal lines. The uncertainty of the energy calibration of the scattering screen is represented by the error bars. (b) Averaged x-ray spectra for the two target types as a semi-logarithmic plot. The prominent K_α (1), B-like (2), and Li-like transitions (3) are indicated. The standard deviation for both target types is shown in gray.

second harmonic scales with the electron density,[29] the strong decrease might be attributed to the lowered plasma density along the structured surface. However, in combination with the reduction of fundamental light reflected from the front surface, it indicates that the energy coupling to the target is enhanced significantly. This observation is consistent with previous studies using structured surface targets.[30,31]

In addition to the strength of the signal, the scattering screens show the 2D profiles of the reflected beam. For the microstructured front, the spot size is slightly bigger and the profile is more homogeneous. Precisely these data and a detailed analysis can be found in the study by Jarrett *et al.*[32]

B. X-ray spectrum

With the improved energy coupling to the target, there are significant changes in the laser-driven radiation and particle source. The x-ray spectrum, shown in Fig. 2(b), shows a significant increase in the spectral intensity when using the structured targets over the flat targets. As a result, the total integrated spectral intensity rises by a factor of 7.3. Furthermore, and more importantly, the central K_α line increases by a factor of 12, and the intensity of higher ionization states observed at energies above 1.8 keV is also enhanced.

The K_α line is produced from a cold and overdense region in the plasma. The ionization is most likely due to electron collisions with some field ionization. Close to the focal spot, the collision rate will be sufficiently high to produce high ionization states, and x-ray radiation is likely to photopump the inner shells, while the initial ionization is due to laser field-induced ionization. The noticeable increase in brightness of both regions suggests that more matter is being ionized by hot electron-ion collisions, and a higher x-ray flux is generated when using the structured targets.[33–36]

The attenuation caused by the filters was included in the data reduction, and the effect of the crystal spectral reflectivity was corrected using the data provided by Henke *et al.*[37] The conversion of the PSL (photo-stimulated luminescence) signal of the image plates to an energy in keV used the findings of Meadowcroft *et al.*[38]

The spectral emission was identified using the collisional-radiative code PrismSPECT.[39]

C. Electron spectrum

The complementary electron spectra show an increase in flux by a factor of 3.1. At the same time, the temperatures obtained using a simple Boltzmann distribution, listed in Table I, show no noticeable change between flat and structured targets. These two observations suggest that most of the additional laser energy absorbed by the microstructured targets is used for generating a higher flux of electrons rather than affecting the temperature. This suggests that extreme field gradients are distributed over a larger area in comparison to flat targets.

D. Proton spectrum

The corresponding proton spectrum derived from the radiochromic film (RCF) data in Fig. 3 shows a similar behavior to the electron spectra in terms of the flux and temperature transitions. The total number of protons increases by a factor of 4.4 using the structured targets instead of the flat targets, while the mean temperature between the target types is comparable at 2.5 ± 0.1 MeV. The spectra recorded with the Thomson parabola agree well with the RCF data.

By attaching a copper mesh (12.7 μm line spacing) to the target back side and analyzing the mesh imprint on the RC film, the proton source size is estimated to be (25 ± 10) μm for flat and (100 ± 10) μm for needle targets in diameter. Protons, being the highest charge-to-mass ratio ion species, are always accelerated first, largely independent of the target material. These protons originate from layers of water vapor or hydrocarbons, which are usually present on the target surface without additional treatment. Protons from this layer on the target surface are exposed to the highest field strengths and screen the electric field for protons and ions from deeper layers. With an expected contamination layer density of $(4\pm1) \times 10^{16}$ protons/cm^2 (Ref. 40) and the approximated source size, the total number of protons in the
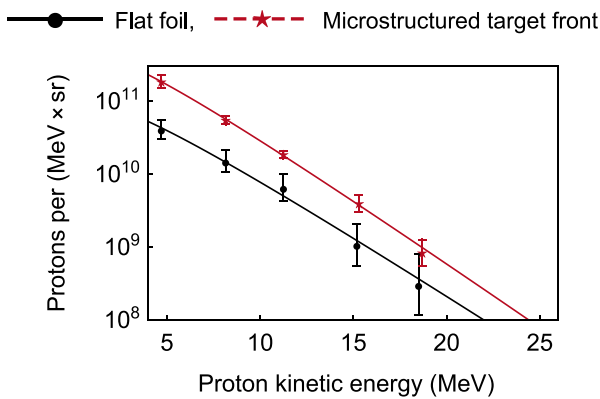
FIG. 3. Combined proton spectra derived from radiochromic film stacks together with the approximated Maxwell distribution. Error bars indicate the standard deviation.

contamination layer on the target rear surface accounts to 2×10^{11} for flat and 3×10^{12} for structured targets. This is in agreement with the number of protons observed. The energy conversion efficiency to protons above 4 MeV accounts to 0.27% for flat and 1.01% for structured targets. Previous studies discussed the effect of surface contaminant depletion,[41,42] and we conclude that the number of protons available in the contamination layer on the rear surface has limited the conversion efficiency.

IV. SIMULATION

In order to get a better understanding of the underlying processes, a series of 2D particle in cell (PIC) simulations were performed with the open-source code EPOCH.[43] The size of the simulation box was $40 \times 20 \, \mu m^2$ with a spatial grid resolution of $40 \times 40 \, nm^2$. The target material was pure hydrogen with an initial density of 10 n_c (with $n_c = \epsilon_0 m_e \omega^2 e^{-2}$ being the critical density), and the boundaries were open for both particles and fields. The laser temporal and spatial profiles were Gaussian with a focal spot size of $10 \, \mu m$ (FWHM), a pulse duration of 100 fs (FWHM), and an intensity of 2×10^{20} W cm^{-2}. This is a very simple approximation of the real Vulcan pulse as the simulated pulse is much shorter, and the prepulse is neglected. In consequence, the expansion of a low density plasma before the arrival of the main peak is not included in the simulations. The laser enters the simulation box from the left at a 0° incidence angle. A total number of 10^9 macroparticles were distributed according to three different simplified geometries, which are shown in Fig. 4(a). The flat target (top) serves as reference. The middle geometry is used to study the effect of electron heating on a tilted surface, while the trough resembles the valleys that are characteristic for the presented microstructures. In the experiment, multiple cones are irradiated simultaneously, and it is difficult to tell which features of the cone-like structures have the greatest impact on their behavior. With this simulation setup, the individual effects arising from the cone shape can be investigated.

The tilted surface demonstrates the effect of an increased surface area onto the electron spectrum, while also including the effect of vacuum heating. The simulation snapshots at 140 fs [Fig. 4(b)] and 180 fs [Fig. 4(c)] after the start of the simulation show that the heating process for the tilted geometry evolves over a longer timescale compared

to the flat one. The larger surface results in the laser driving a larger number of electrons, which can be seen in the spectra shown in Fig. 4(d) (at 100 fs) and Fig. 4(e) (at 200 fs). The inclusion of vacuum heating seems to play a role in countering the effects of the decreased intensity and might be one reason why the temperature of the electrons stays comparable. Under the displayed geometric conditions, the electrons are partially driven into the target by the field component perpendicular to the surface, which leads to a wider electron spread.

Specifically, the pointed troughs make the presented structures unique. The total increase in the exposed surface area is in general multiple times larger than for a flat, tilted target. Therefore, the total number of heated electrons is further enhanced, as can be seen in Fig. 4(e). Here, vacuum heating can occur as well, such that the lower surface energy density flux can be partially compensated. Additionally, the light that is lost in both the flat and tilted geometries due to reflection will interact with the opposite surface as well. Therefore, the overall amount of absorbed energy can be increased. Another aspect is the coupling of the electrons to the laser in an almost collisionless region, which optimizes the energy transfer. This was also previously reported by Blanco et al.[16] As their structure size is comparable to the laser wavelength, the effect of the tilted surface is significantly weaker.

The time evolution in Figs. 4(a)–4(c) shows that the trough has the longest heating over the depicted timescale. Also, the electron spread is the widest, which explains the increased source size of the particles accelerated from the rear side.

V. DISCUSSION

This is the first report of the use of silicon targets with cone-like microstructures, which show highly light-absorbing properties in high power laser experiments. Here, we have presented a comparison of flat and microstructured monocrystalline silicon under high-contrast and high-intensity irradiation.

The reflection of laser light from the target front is reduced, which might indicate a better laser-to-target coupling for structured targets. The more important aspect, however, is the difference in the energy transfer processes, which was studied with a series of 2D PIC simulations. A flat surface was compared to a tilted target and a trough, which is characteristic for the presented structures.

Even though the laser prepulse in the experiment is cleaned with a double plasma mirror system, a slight expansion of an underdense plasma due to laser irradiation prior to the arrival of the main pulse is likely. However, the surface structure will remain cone-like as long as the plasma scale length is in the micrometer range. The surface area of the cold target is seven times larger, so depending on this scale length, the peak intensity is lowered by up to 80%. Our results show an increased number of electrons heated by the laser, which can be explained by the enlarged surface.

At the same time, the electron temperature of flat and structured targets is similar, which is probably caused by a combination of several phenomena: The sloped surfaces promote vacuum heating as can be seen in the simulations. However, without a sharp matter vacuum boundary, the impact of this mechanism diminishes. Nonetheless, with the existence of an underdense plasma, the electron heating can benefit from laser absorption processes such as resonance absorption. In addition, the light gets trapped in the troughs, and the sharp tips of the microstructures minimize the amount of directly back reflected
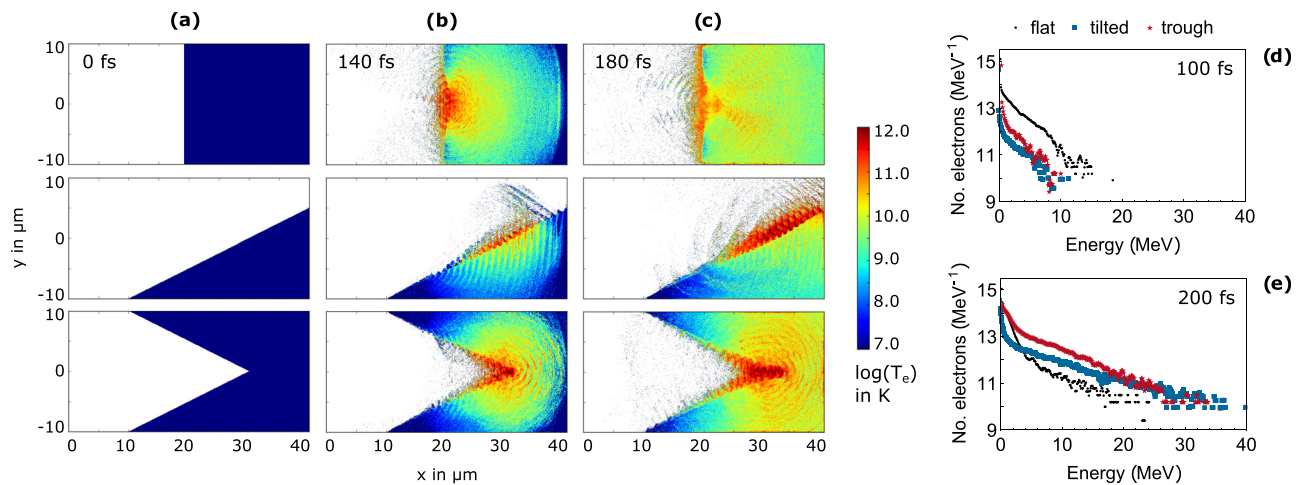
FIG. 4. Simulated electron temperatures T_e for three different target geometries at (a) 0 fs, (b) 140 fs, and (c) 180 fs after simulation start. At the top, a flat reference target is shown. The middle row depicts a tilted target, while the bottom row corresponds to the surface geometry of a trough between two microstructures. For the latter, the heated region is much longer existent, and the electrons show a wider opening angle. The color bar denotes $\log(T_e)$ in K. The electron spectrum is shown in the subfigure (d) at 100 fs and (e) 200 fs. While the electron number and cut-off energy of the flat target are higher at early times, the tilted and trough geometry dominate at later stages. At both snapshots, the trough performs better than the tilted target.

light, which is opposed to other presented microstructures.[44] The triangular geometry also builds vacuum gaps for almost collisionless electron heating. The combination of these effects counteracts the decrease in laser intensity, such that the electron temperatures are unchanged. This applies both to the experiment and the simulation, although the coupling to a low density preplasma between the gaps is neglected in the latter.

One of the most important results is the boost in spectral x-ray emission. The spectrum shows a rise in the signal of K_α and higher ionization states when switching from flat to microstructured targets. This suggests that more electrons are heated during the laser interaction with the microstructured target. Since the K_α cross section has a peak at electron energies in the keV range,[45] the increased number of low energy electrons especially leads to an enhanced emission. Particularly, for experiments using x-ray backlighters as the secondary source, the amplification of a specific emission line is of great interest.[9] The measured proton source size can be used to normalize the x-ray intensity. With this correction, the x-ray energy flux per source area decreases for the microstructured targets by a factor of 2.

We suspect that the observed increase in the proton number is limited by the number of available protons in the contamination layer on the target back side. For future experiments, we suggest an artificial hydrogen-rich layer on the target back side to further increase the flux of protons and therefore the conversion efficiency. Furthermore, a combination of the structured target front with a confined piece of material with energetic x-ray lines could produce an intense point size source of high energetic x-ray line emission photons.

VI. CONCLUSION

In conclusion, our experiments show that the employment of cone-shaped microstructures enhances the laser-to-target coupling. We observe a 7.3× rise in overall x-ray intensity and a 12× boost of the silicon K_α line. The electron and proton fluxes are increased by a factor of 3.1 and 4.4, respectively, while their temperatures stay constant in comparison to flat foil targets. The reflected light is reduced by a factor of 3. We complement the experimental results with a series of 2D PIC simulations, which indicate that the cone-shape in particular makes the presented structures remarkable. Their increased surface and the modification of the electron heating process with regard to resonance absorption and vacuum heating are essential for the improvement.

REFERENCES

[1]S. Wilks, W. Kruer, M. Tabak, and A. Langdon, Phys. Rev. Lett. **69**, 1383 (1992).
[2]P. Bolton, K. Parodi, and J. Schreiber, *Applications of Laser-Driven Particle Acceleration* (CRC Press, Boca Raton, 2018).
[3]A. Macchi, M. Borghesi, and M. Passoni, Rev. Mod. Phys. **85**, 751 (2013).
[4]O. Klimo, J. Psikal, J. Limpouch, J. Proska, F. Novotny, T. Ceccotti, V. Floquet, and S. Kawata, New J. Phys. **13**, 053028 (2011).
[5]G. Cristoforetti, P. Londrillo, P. Singh, F. Baffigi, G. D'Arrigo, A. D. Lad, R. Milazzo, A. Adak, M. Shaikh, D. Sarkar, G. Chatterjee, J. Jha, M. Krishnamurthy, G. Kumar, and L. Gizzi, Sci. Rep. **7**, 1479 (2017).
[6]A. Lübcke, A. A. Andreev, S. Höhm, R. Grunwald, L. Ehrentraut, and M. Schnürer, Sci. Rep. **7**, 44030 (2017).

[7]Z. Zhao, L. Cao, L. Cao, J. Wang, W. Huang, W. Jiang, Y. He, Y. Wu, B. Zhu, K. Dong, Y. Ding, B. Zhang, Y. Gu, M. Y. Yu, and X. T. He, Phys. Plasmas **17**, 123108 (2010).

[8]W. Yan, C. Fruhling, G. Golovin, D. Haden, J. Luo, P. Zhang, B. Zhao, J. Zhang, C. Liu, M. Chen, S. Chen, S. Banerjee, and D. Umstadter, Nat. Photonics **11**, 514 (2017).

[9]D. H. Kalantar, S. W. Haan, B. A. Hammel, C. J. Keane, O. L. Landen, and D. H. Munro, Rev. Sci. Instrum. **68**, 814 (1997).

[10]F. Raksi, K. R. Wilson, Z. Jiang, A. Ikhlef, C. Y. Côté, and J.-C. Kieffer, J. Chem. Phys. **104**, 6066 (1996).

[11]M. Dozières, G. Petrov, P. Forestier-Colleoni, P. Campbell, K. Krushelnick, A. Maksimchuk, C. McGuffey, V. Kaymak, A. Pukhov, M. Capeluto, R. Hollinger, V. Shlyaptsev, J. Rocca, and F. Beg, Plasma Phys. Controlled Fusion **61**, 065016 (2019).

[12]R. Hollinger, C. Bargsten, V. N. Shlyaptsev, V. Kaymak, A. Pukhov, M. G. Capeluto, S. Wang, A. Rockwood, Y. Wang, A. Townsend, A. Prieto, P. Stockton, A. Curtis, and J. J. Rocca, Optica **4**, 1344 (2017).

[13]P. McKenna, D. Carroll, O. Lundh, F. Nürnberg, K. Markey, S. Bandyopadhyay, D. Batani, R. Evans, R. Jafer, S. Kar, D. Neely, D. Pepler, M. Quinn, R. Redaelli, M. Roth, C.-G. Wahlström, X. Yuan, and M. Zepf, Laser Part. Beams **26**, 591–596 (2008).

[14]A. Andreev, N. Kumar, K. Platonov, and A. Pukhov, Phys. Plasmas **18**, 103103 (2011).

[15]M. Borghesi, Nucl. Instrum. Methods Phys. Res., Sect. A **740**, 6 (2014).

[16]M. Blanco, M. Flores-Arias, C. Ruiz, and M. Vranic, New J. Phys. **19**, 033004 (2017).

[17]T.-H. Her, R. J. Finlay, C. Wu, S. Deliwala, and E. Mazur, Appl. Phys. Lett. **73**, 1673 (1998).

[18]B. Franta, D. Pastor, H. H. Gandhi, P. H. Rekemeyer, S. Gradečak, M. J. Aziz, and E. Mazur, J. Appl. Phys. **118**, 225303 (2015).

[19]X. Liu, P. R. Coxon, M. Peters, B. Hoex, J. M. Cole, and D. J. Fray, Energy Environ. Sci. **7**, 3223 (2014).

[20]M. Shen, C. H. Crouch, J. E. Carey, and E. Mazur, Appl. Phys. Lett. **85**, 5694 (2004).

[21]I. Gnilitskyi, T. J.-Y. Derrien, Y. Levy, N. M. Bulgakova, T. Mocek, and L. Orazi, Sci. Rep. **7**, 8485 (2017).

[22]C. Wu, C. Crouch, L. Zhao, J. Carey, R. Younkin, J. Levinson, E. Mazur, R. Farrell, P. Gothoskar, and A. Karger, Appl. Phys. Lett. **78**, 1850 (2001).

[23]T. Ebert, N. W. Neumann, T. Abel, G. Schaumann, and M. Roth, High Power Laser Sci. Eng. **5**, e13 (2017).

[24]C. Hernandez-Gomez, P. Brummitt, D. Canny, R. Clarke, J. Collier, C. Danson, A. Dunne, B. Fell, A. Frackiewicz, S. Hancock, S. Hawkes, R. Heathcote, P. Holligan, M. Hutchinson, A. Kidd, W. Lester, I. Musgrave, D. Neely, D. Neville, P. Norreys, D. Pepler, C. Reason, W. W. T. Shaikh, and B. Wyborn, J. Phys. IV **133**, 555–559 (2006).

[25]E. Martinolli, M. Koenig, J. M. Boudenne, E. Perelli, D. Batani, and T. A. Hall, Rev. Sci. Instrum. **75**, 2024 (2004).

[26]D. Rusby, L. Wilson, R. Gray, R. Dance, N. Butler, D. MacLellan, G. Scott, V. Bagnoud, B. Zielbauer, P. McKenna, and D. Neely, J. Plasma Phys. **81**, 5 (2015).

[27]R. J. Gray, X. H. Yuan, D. C. Carroll, C. M. Brenner, M. Coury, M. N. Quinn, O. Tresca, B. Zielbauer, B. Aurand, V. Bagnoud, J. Fils, T. Kühl, X. X. Lin, C. Li, Y. T. Li, M. Roth, D. Neely, and P. McKenna, Appl. Phys. Lett. **99**, 171502 (2011).

[28]C. Ziener, P. Foster, E. Divall, C. Hooker, M. Hutchinson, A. Langley, and D. Neely, J. Appl. Phys. **93**, 768 (2003).

[29]K. P. Singh, D. N. Gupta, S. Yadav, and V. K. Tripathi, Phys. Plasmas **12**, 013101 (2005).

[30]D. Margarone, O. Klimo, I. J. Kim, J. Prokůpek, J. Limpouch, T. M. Jeong, T. Mocek, J. Pšikal, H. T. Kim, J. Proška, K. H. Nam, L. Štolcová, I. W. Choi, S. K. Lee, J. H. Sung, T. J. Yu, and G. Korn, Phys. Rev. Lett. **109**, 234801 (2012).

[31]S. Jiang, A. Krygier, D. Schumacher, K. Akli, and R. Freeman, Phys. Rev. E **89**, 013106 (2014).

[32]J. Jarrett, M. King, R. J. Gray, N. Neumann, L. Döhl, C. D. Baird, T. Ebert, M. Hesse, A. Tebartz, D. R. Rusby, N. Woolsey, D. Neely, M. Roth, and P. McKenna, High Power Laser Sci. Eng. **7**, e2 (2019).

[33]D. Salzmann, C. Reich, I. Uschmann, E. Förster, and P. Gibbon, Phys. Rev. E **65**, 036402 (2002).

[34]J. Colgan, J. Abdallah, A. Y. Faenov, S. A. Pikuz, E. Wagenaars, N. Booth, O. Culfa, R. J. Dance, R. G. Evans, R. J. Gray, T. Kaempfer, K. L. Lancaster, P. McKenna, A. L. Rossall, I. Y. Skobelev, K. S. Schulze, I. Uschmann, A. G. Zhidkov, and N. C. Woolsey, Phys. Rev. Lett. **110**, 125001 (2013).

[35]S. B. Hansen, J. Colgan, A. Y. Faenov, J. Abdallah, S. A. Pikuz, I. Y. Skobelev, E. Wagenaars, N. Booth, O. Culfa, R. J. Dance, G. J. Tallents, R. G. Evans, R. J. Gray, T. Kaempfer, K. L. Lancaster, P. McKenna, A. K. Rossall, K. S. Schulze, I. Uschmann, A. G. Zhidkov, and N. C. Woolsey, Phys. Plasmas **21**, 031213 (2014).

[36]S. Pikuz, A. Faenov, J. Colgan, R. Dance, J. Abdallah, E. Wagenaars, N. Booth, O. Culfa, R. Evans, R. Gray, T. Kaempfer, K. Lancaster, P. McKenna, A. Rossall, I. Skobelev, K. Schulze, I. Uschmann, A. Zhidkov, and N. Woolsey, High Energy Density Phys. **9**, 560 (2013).

[37]B. L. Henke, E. M. Gullikson, and J. C. Davis, At. Data Nucl. Data Tables **54**, 181 (1993).

[38]A. Meadowcroft, C. Bentley, and E. Stott, Rev. Sci. Instrum. **79**, 113102 (2008).

[39]J. MacFarlane, I. Golovkin, P. Woodruff, D. Welch, B. Oliver, T. Mehlhorn, and R. Campbell, in Proceedings of the Inertial Fusion and Sciences Applications (2003), Vol. 457.

[40]G. Hoffmeister, C. Bellei, K. Harres, D. Ivanov, D. Kraus, A. Pelka, B. Rethfeld, G. Schaumann, and M. Roth, Phys. Rev. Spec. Top.-Accel. Beams **16**, 041304 (2013).

[41]R. A. Snavely, M. H. Key, S. P. Hatchett, T. E. Cowan, M. Roth, T. W. Phillips, M. A. Stoyer, E. A. Henry, T. C. Sangster, M. S. Singh, S. C. Wilks, A. MacKinnon, A. Offenberger, D. M. Pennington, K. Yasuike, A. B. Langdon, B. F. Lasinski, J. Johnson, M. D. Perry, and E. M. Campbell, Phys. Rev. Lett. **85**, 2945 (2000).

[42]M. Roth, A. Blazevic, M. Geissel, T. Schlegel, T. E. Cowan, M. Allen, J.-C. Gauthier, P. Audebert, J. Fuchs, J. Meyer-Ter Vehn, M. Hegelich, S. Karsch, and A. Pukhov, Phys. Rev. ST Accel. Beams **5**, 061301 (2002).

[43]T. D. Arber, K. Bennett, C. S. Brady, A. Lawrence-Douglas, M. G. Ramsay, N. J. Sircombe, P. Gillies, R. G. Evans, H. Schmitz, A. R. Bell, and C. P. Ridgers, Plasma Phys. Controlled Fusion **57**, 113001 (2015).

[44]M. Sedov, A. Y. Faenov, A. Andreev, I. Y. Skobelev, S. Ryazantsev, T. Pikuz, P. Durey, L. Doehl, D. Farley, C. Baird, K. Lancaster, C. Murphy, N. Booth, C. Spindloe, P. Platonov, P. McKenna, R. Kodama, N. Woolsey, and S. Pikuz, Laser Part. Beams **37**, 176 (2019).

[45]M. Liu, Z. An, C. Tang, Z. Luo, X. Peng, and X. Long, At. Data Nucl. Data Tables **76**, 213 (2000).